



# Rapid fabrication of ultra-fine grain intermetallic compound powder in milliseconds under ultrasonic vibrations

Luyao Li, Wenxin Wen, Jinbiao Huang, Jianan Fu, Jiang Ma \*

Shenzhen Key Laboratory of High Performance Nontraditional Manufacturing, College of Mechatronics and Control Engineering, Shenzhen University, Shenzhen, 518060, China

## ARTICLE INFO

### Keywords:

Powder fabrication  
Ultrasonic vibration treatment  
Ultra-fine grain  
Crystallized metallic glasses  
Fatigue crack nucleation

## ABSTRACT

As a key raw material for industrial production and scientific research, intermetallic compounds (IMCs) powder has broad application prospects, and it has a performance breakthrough in its nanocrystalline state. Crystallized metallic glasses (MGs) are a class of IMCs, its powder has great potentials for electromagnetic conversion, catalysis, exhaust treatment and biomedical application. Although many powder fabrication methods exist, a simple, fast method to prepare ultra-fine grain IMC powders is still being pursued. Here we report a facile method to fabricate ultra-fine grain (<5 nm) crystallized MGs powder by ultrasonic vibration treatment (UVT). At room temperature and well below the ultimate material strength, UVT can rapidly breaks bulk crystallized MGs down to micron and nanoscale powders. Compared to other methods, UVT has an outstanding time advantage in within 60 s (1000 times faster than the ball milling). The experimental show that UVT causes rapid grain refinement in crystallized MGs, inducing fatigue crack nucleation at the grain boundaries (GBs) and then smash in milliseconds. Our results provide a fast and cost-efficient method for the production of micro and nano scale ultra-fine grain IMC powders.

## 1. Introduction

With the progress of technology, IMCs powder has been developed and applied in metallurgy [1], chemical industry [2], energy storage materials [3], semiconductors [4], magnetic materials [5], super-conducting materials [6], sensors [7], 3D printing [8,9] etc., showing good application prospects. At the same time, nanograin structure can greatly improve the properties of the IMCs, such as mechanical properties [10], catalytic ability [11] and magnetic properties [12]. However, it is very difficult to obtain ultra-fine crystal structure. Therefore, nanocrystalline IMCs powder preparation technology is a key issue in the current research in the field of materials, and the development of new technologies in this field has a broad development prospect. Crystallized MG are a class of IMCs with important application prospects, and its powders have broad applications. For example, the Fe-based crystallized MG powder can be used in the field of electromagnetic [12,13], the precious metal-based in the field of catalysis [14–16], the rare earth-based in the treatment of automobile exhaust gas [17,18], the Mg-based in biomedical application [19], etc.

At present, the methods of preparing metal powders are divided into mechanical, physical and physical-chemical methods. The most

representative of the mechanical method is the ball milling method [20–22], which is widely used to manufacture ultra-fine grain metal and metal-based composite powders. However, this method is too time-consuming, usually taking hours to days to obtain the powder, and impurities may be introduced. Physical methods include a variety of atomization methods [23,24]. This method is cost effective and particle size controllable, but it will change the state of the material [23]. The physical-chemical methods include deposition [25–27] and electrolysis [28–30], which are commonly used to produce high purity, but the production cost is expensive and the yield needs to be improved. Although quite a few of the above methods have been applied in practice, there are still two key problems: inefficiency [20,25,30] and high cost [25,29]. Therefore, an efficient and low-cost method for powder production is still being pursued.

Here we report an ultra-fast method of powder preparation at room temperature - powder fabrication under UVT. In this work, the ultrasonic vibrations (20,000 Hz) can cause crystallized MGs to be crushed to the micron and even nanometer level at room temperature and low stress (20 MPa) in ribbon or bulk states conveniently. Meanwhile, the powder obtained by UVT exhibits ultra-fine grain state. Compared with other methods, the UVT method has apparent time advantages (within 1

\* Corresponding author.

E-mail address: [majiang@szu.edu.cn](mailto:majiang@szu.edu.cn) (J. Ma).

<https://doi.org/10.1016/j.intermet.2022.107672>

Received 28 April 2022; Received in revised form 12 July 2022; Accepted 22 July 2022

0966-9795/© 2022 Elsevier Ltd. All rights reserved.

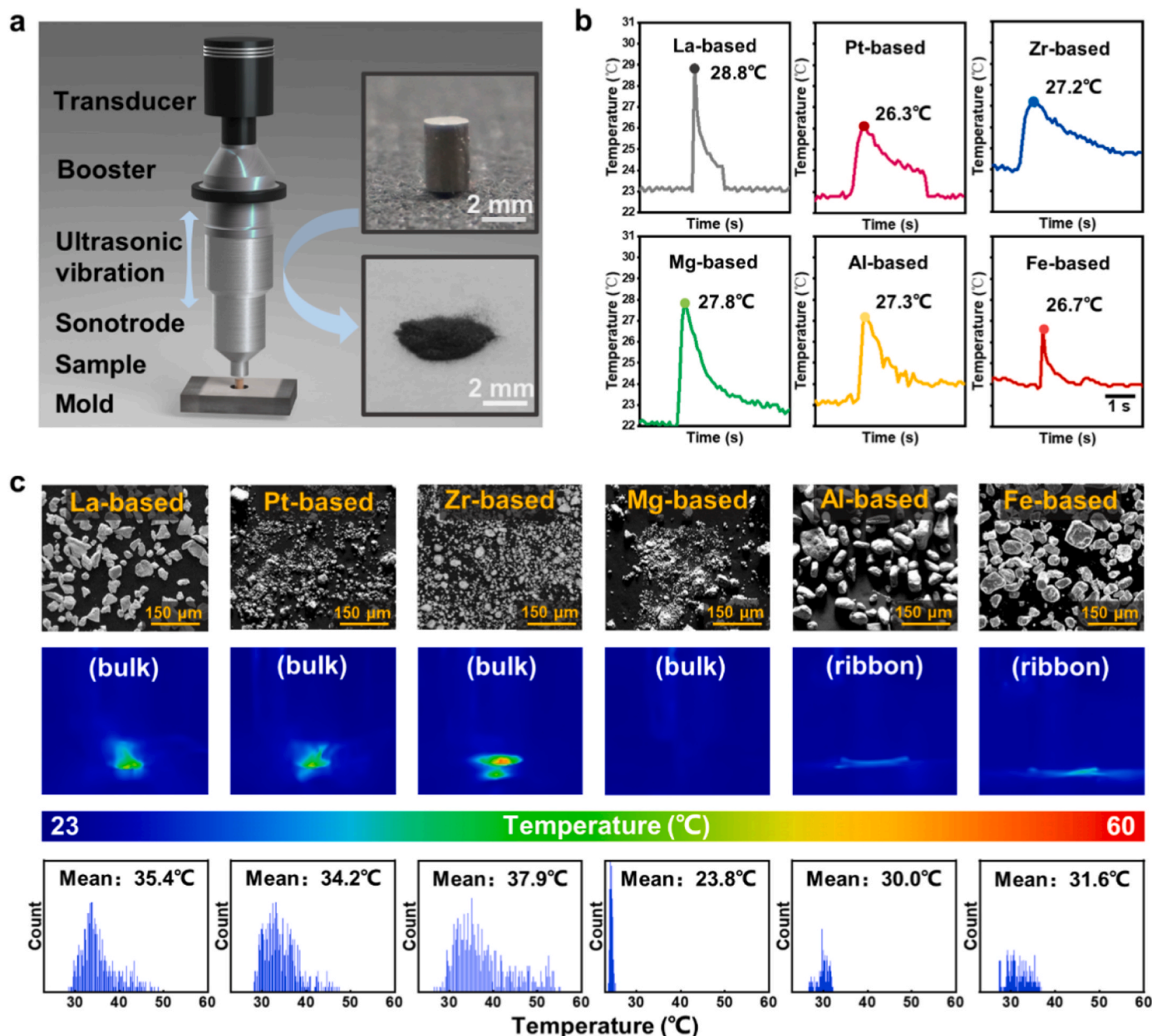


**Fig. 1.** (a) The schematic diagram of UVT. (b) The time-temperature profile during each powder beating. (c) The SEM images of all powders. Below is its corresponding temperature distribution image and temperature numerical distribution when the bulk crystallized MGs crushing.

min) and guaranteed yield. In particular, the powder fabrication under UVT is over 1000 times faster compared to the ball milling method [22]. The experimental results show that crystallized MGs rapidly extreme grain refinement and cracks nucleate at the grain triple junction under UVT, which is the reason why crystallized MGs can be crushed into small particles efficiently and exhibits an ultra-fine grain state (<5 nm). The present work provides a groundbreaking method for the facile and mass production of IMC powders.

## 2. Material and methods

The compositions of  $\text{La}_{55}\text{Al}_{25}\text{Ni}_5\text{Cu}_{10}\text{Co}_5$ ,  $\text{Zr}_{65}\text{Cu}_{17.5}\text{Ni}_{10}\text{Al}_{7.5}$ ,  $\text{Fe}_{78}\text{Si}_9\text{B}_{13}$ ,  $\text{Mg}_{65}\text{Cu}_{25}\text{Y}_{10}$ ,  $\text{Al}_{89}\text{Ni}_6\text{La}_5$  and  $\text{Pt}_{57.5}\text{Cu}_{14.7}\text{Ni}_{5.3}\text{P}_{22.5}$  crystallized MGs were selected as the raw materials for this experiment. The La-based, Zr-based, Mg-based, and Pt-based MGs were prepared by casting pure monomers (>99.99% purity) into bulks by conventional water-cooled copper molds under a low-pressure vacuum environment with

inert gas argon. Al-based and Fe-based were prepared in ribbon state using water-cooled rotating copper die. A vacuum resistance furnace was used to crystallize the MGs, and the MGs were heated to 100 °C above the crystallization temperature ( $T_x$ ) and held for 40 min. The prepared bulk material with 2 mm diameter was cut into 3 mm long pieces (1:1.5) for comparison of loads under ultrasonic vibration and compression tests.

The ultrasonic vibration device was used to crush crystallized MGs with a vibration frequency of 20 kHz and a maximum power of 2500 W. The schematic diagram of the device is shown in Fig. 1a. The ultrasonic device consists of a transducer (converts electrical energy into vibration), a booster (amplifies the amplitude of vibration) and a sonotrode (transmits mechanical vibration to the sample). The mechanism is very different compared to other ultrasonic related treatments. In this UVT experiment, the sonotrode comes in contact with the sample under the trigger force, and then starts to vibrate at a fixed amplitude. UVT was divided into two processes: bulk fracture process and powder beating

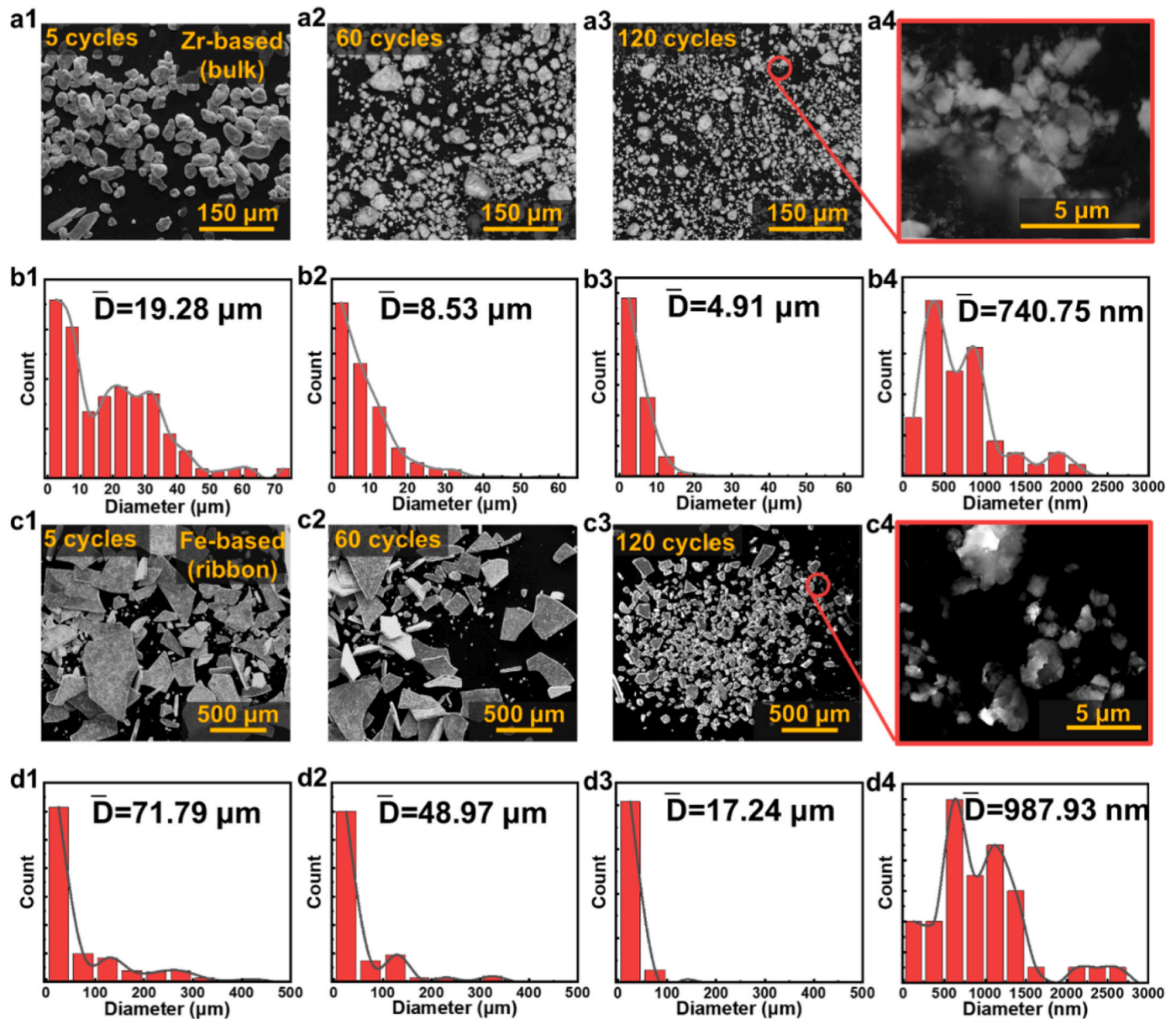


Fig. 2. Characterization of powders. (a1-a4) The SEM images of Zr-based powders: 5-cycle, 60-cycle, 120-cycle and nanoparticle samples. (b1-b4) The Particle size analysis images of Zr-based powders corresponds to (a1-a4). (c1-c4) The SEM images of Fe-based powders: 5-cycle, 60-cycle, 120-cycle and nanoparticle samples. (d1-d4) The particle size analysis images of Fe-based powders correspond to (c1-c4).

process. The fracture process was used to observe the temperature and stress of bulk fracture under UVT (for comparison with the static compression test), and device will stop acting when the sample fracture. The beating process was set to release 100 J energy to beat once for one cycle (time duration 0.5 s), and 5, 60 and 120 cycles were processed respectively (cycle as a variable).

Cylindrical specimens (3 mm in length and 2 mm in diameter) with a length/diameter ratio of 1.5 were compressed (strain rate of  $0.001 \text{ s}^{-1}$ ) by Z050TEW at room temperature according to ASTM Standard [31]. A self-made force gauge was used to perform load measurements at UVT, and the data was transferred to a computer using a data acquisition card (National Instruments NI-9237) with a sampling frequency of 1000 Hz. An infrared imager (Fotric 280d) was used to detect thermal images of the bulk fracture process. Due to the enclosed environment of the powder beating process, its temperature measurement was performed using a homemade thermocouple and a data acquisition card. Scanning electron microscopy (SEM; Fei quanta FEG 450) was used to observe the

powders and bulks cross-sectional morphology. Transmission Electron Microscope (TEM, Fei Titan Themis) with its mounted energy dispersive spectroscopy (EDS) was used to observe the structural information of the samples. A high-speed video camera was used to capture the crushing process of crystallized bulk MG, and the video screen playback was slowed down by 160 times compared to the actual situation.

### 3. Results and discussion

Fig. 1a shows the schematic diagram of the ultrasonic vibration device. In our previous work, UVT was used for cold jointing MG [32–34] and alloy modification [35]. The whole UVT process is very simple, the crystallized MGs was placed in a fixed mold and then the material was crushed by applying ultrasonic vibrations to the sample through the sonotrode. High-speed camera was used to capture the motion of Zr-based bulk crushing (Video S1 in the Supplementary Materials), which can be crushed in 0.2 s. After that, 5, 60 and 120 cycles (time

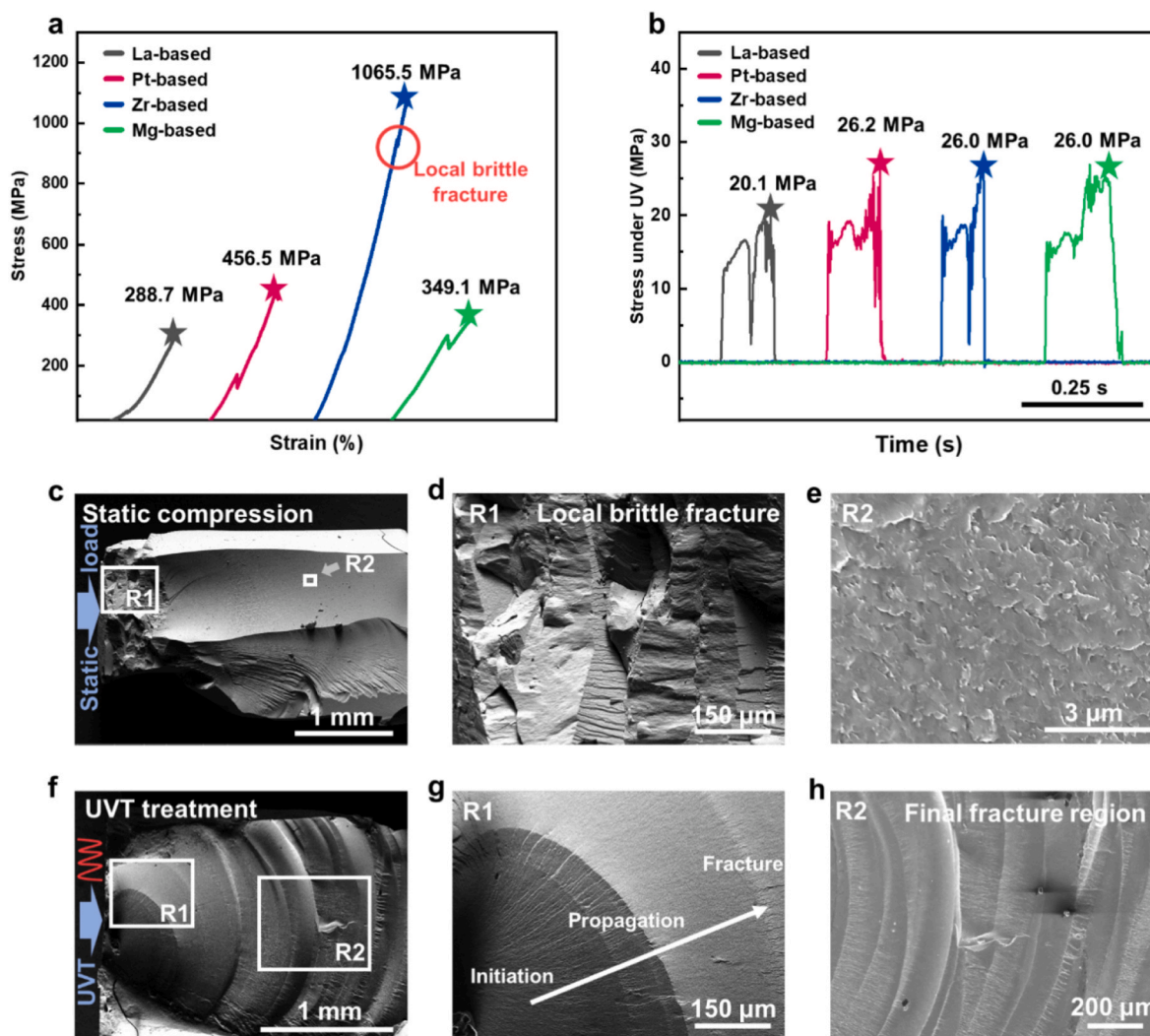


**Fig. 3.** (a) The stress-strain curve of bulk crystallized MGs under static compression. (b) The stress-time curve of bulk crystallized MGs under UVT. (c) The morphology of the fracture surface of Zr-based crystallized MGs under static compression. (d–e) The morphology of the fracture surface corresponding to the selected regions R1 and R2 in (c). (f) The morphology of the fracture surface of Zr-based crystallized MGs under UVT. (g–h) The morphology of the fracture surface corresponding to the selected regions R1 and R2 in (f).

consume 2.5, 30 and 60 s respectively) of beating were performed on the powders of each materials, respectively. To explore the overall temperature change during the UVT process, thermocouples were used to measure the powder temperature during one cycle (Fig. 1b). It is worth noting that whatever the composition of the powder, it is at room temperature condition during the UVT process, and the maximum temperature does not exceed 30 °C. To further precisely demonstrate the room temperature nature of UVT, the thermal imager was used to capture the temperature distribution at the moment of bulks or ribbons breaking, which can be seen Fig. 1c. The results show that the bulk samples have a slightly higher temperature than the ribbons, and the highest temperature found in the Zr-based IMCs has an average temperature of only 37.9 °C, with a maximum local temperature of 53 °C. The ribbons show a lower temperature distribution, with an average temperature of 31.6 °C and a maximum temperature of 37 °C for the Fe-based, for example. On the one hand, it is duo to the ribbon is too thinner and has a larger area subjected to UVT, while the bulk has a smaller contact area and the UVT is more concentrated in the sample (Fig. S1 in the Supplementary Materials), so the temperature is slightly higher. On the other hand, the temperature is also related to the nature of the material. We counted the energy released by the ultrasonic device to crush the 4 bulk samples, the result show that crush Zr-based

crystallized MG (the sample with highest strength and temperature) requires release the most energy (Fig. S2 in the Supplementary Materials).

Supplementary video related to this article can be found at <https://doi.org/10.1016/j.intermet.2022.107672>

In this work, six kinds of powders with different compositions were fabricated: La-based, Zr-based, Mg-based, Pt-based (raw material as bulks) and Al-based, Fe-based crystallized MGs (raw material as ribbons). In order to further investigate the situation of the powder obtained by UVT, SEM was used to observe the microscopic morphology of the powders and also to analyze the particle size of the obtained results, as shown in Fig. 2. In the case of Zr-based bulk materials, the powder treated with UVT for 5 cycles has a wide range of particle size distribution (10–50 μm), with a statistical average of 19.28 μm (Fig. 2a1 and b1). The 60 cycles powder is shown in Fig. 2a2, and the particle size analysis (Fig. 2b2) shows a further reduction of the large-particle powder (mostly below 20 μm), with an average particle size of 8.53 μm. The 120 cycles powder particle size was substantially reduced (Fig. 2a3), while the particle distribution became more uniform (mostly below 10 μm) (Fig. 2b3), with an average particle size of 4.91 μm. Notably, further analysis of the 120 cycles powder revealed the presence of a large number of nanoscale powders (Fig. 2a4 and b4), which average particle

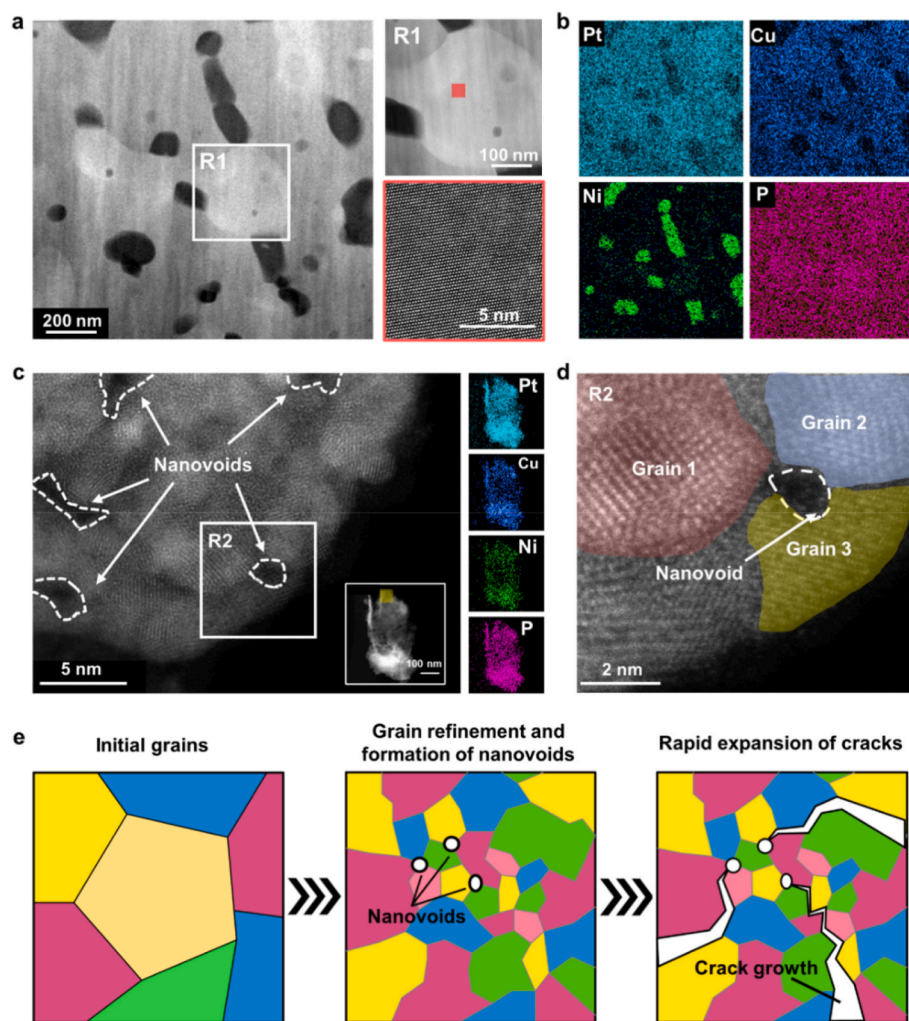


Fig. 4. (a) The microstructure of raw bulk Pt-based crystallized MG. The inset in the upper right corner shows a zoomed-in view of a single grain in the region R1. The inset in the lower right corner shows the arrangement of atoms within this grain (corresponding to the red area). (b) EDS analysis of the raw bulk Pt-based crystallized MG. (c) Local STEM image of the Pt-based powder sample made by UVT (corresponding to the yellow region in the inset), which has a large number of nano hollows. The EDS image of the powder is shown on the right. (d) The STEM image of nano hollow situation in the selected regions R2 in (c). (e) Schematic diagram of the crushing mechanism of IMCs under ultrasonic vibration, in which different colors represent different grain orientations.

size is 740.75 nm. The powder prepared from ribbons as raw material has larger particle size compared to the bulk. In the case of the Fe-based crystallized MGs, the particle size of the 5 cycles powder is a large lamellar structure, with high number of particles with different sizes (below 400  $\mu\text{m}$ , with an average particle size of 71.19  $\mu\text{m}$ ) (Fig. 2c1 and d1). The particle size of the 60 cycles powder was further reduced, mostly below 300  $\mu\text{m}$ , with an average particle size of 48.97  $\mu\text{m}$  (Fig. 2c2 and d2). The particle size distribution of the 120 cycles powder became more uniform too, mostly below 50  $\mu\text{m}$ , with an average particle size of 17.24  $\mu\text{m}$  (Fig. 2c3 and d3). Meanwhile, considerable amount of nanoscale powder is also present in 120 cycles powder (Fig. 2c4 and d4), which average particle size is 987.93 nm. In addition, the Al-based, La-based, Pt-based and Mg-based have the same rule, see Fig. S3 in the Supplementary Materials. The above results show that the powder particle size fabricated by bulk form are smaller than that of fabricated by ribbons. It is duo to the ribbon is thinner (20  $\mu\text{m}$ ) and has a larger contact surface with the sonotrode, which results the UVT not as concentrated as the bulk samples and fine powder manufacturing needs more time. And it is worth noting that the powder prepared from the same type of raw material (bulk or ribbon) will eventually show a relatively similar particle size distribution. In summary, as the particle size is further reduced and homogenized with the increase of processing cycle, it can be considered that UVT is a highly efficient powder manufacturing method. This method not only prepare homogeneous powder efficiently and quickly, but even prepare nanoscale particles.

To further verify the availability of the UVT method, the mass of the fabricated powder was measured. The maximum mass of powders is

determined by the size of the sonotrode and mold, and the larger size of instrument can manufacture more powders. Fig. S4 in the Supplementary Materials shows two different sizes of instruments (10 mm diameter and 50 mm diameter). We fabricated almost 13.77 g Zr-based powders at once by used 50 mm diameter instrument.

To further investigate the mechanism of UVT action on crystallized MGs, we observed the strength comparison of samples under UVT and static compression. Since the ribbons could not be subjected to compression experiments, so four types of bulk raw materials were analyzed in this work. The results show that under static compression, the bulk crystallized MGs all exhibit high strengths, with the highest strengths of 288.7 MPa, 456.5 MPa, 1065.5 MPa, and 349.1 MPa for La-based, Pt-based, Zr-based, and Mg-based, respectively (Fig. 3a). In this case, there is a 'fold' in the compression curve, which can be considered as a local area of brittle fracture. However, under the force of UVT (Fig. 3b), all materials exhibit similarly low strengths (maximum 26 MPa) in contrast to the case of static compression. The difference in fracture strength between the two cases is enormous, especially for bulk Zr-based crystallized MGs, which are 40 times smaller under UVT than under static compression.

To further investigate the mechanism of low stress, the SEM was used to research the microscopic morphology of the fracture surface. Fig. 3c shows the flat fracture surface of the Zr-based bulk crystallized MGs under conventional static compression. Localized brittle fracture (Fig. 3d) occurs in the loaded region, which is the reason for the 'fold' in the stress-strain curve (Fig. 3a). We observed the fracture morphology of the flat area (Fig. 3e), which is consistent with the size of phase

distribution in the raw material (Fig. S5 in the Supplementary Materials). So it is clearly a brittle fracture along the crystal. The fracture surface of the Zr-based bulk crystallized MGs under UVT is shown in Fig. 3f, which has obvious fatigue cracks, different from static compression. The surface has obvious fatigue initiation area, crack propagation area and fracture area (Fig. 3g and h), and the fatigue initiation is located on the side near the sonotrode. The above results indicate that ultrasonic vibration rapidly excites fatigue crack nucleation crystallized MG.

To further investigate the mechanism of this difference, the microstructures of bulk Pt-based crystallized MGs and its powders were observed under TEM. TEM images of the raw bulk material show regular grains (100–500 nm) and neat atomic structure (Fig. 4a). The EDS results show that these grains are interspersed with part of dispersed Ni-rich phases (Fig. 4b). The STEM mode was used to observe the atomic structure morphology of the powder, as shown in Fig. 4c. The powder obtained by UVT has all grains below 5 nm and numerous GBs. More noteworthy is the presence of high number of nanovoids in the sample. Fig. 4d represents a local magnified image of one of the nanovoids (square area R2) in Fig. 4c, which shows that the nanovoid appears at the junction of three ultra-fine grains.

Fatigue life consists mainly of crack initiation and propagation, and studies have shown that most of the cycles are used for initiation [36]. Different deformation mechanisms exist in nanocrystals of different sizes [37–39]: in the diameter range of 100–500 nm, the deformation mechanisms are similar to those of small-grained conventional materials (dominated by dislocation). For diameters smaller than 10 nm, slip at GBs is the dominant mode of deformation. Typically, grain reduction to 100 nm leads to an increase in strength; grain size reduction below 20 nm leads to a decrease in strength, which is referred to as Hall-Petch breakdown [40,41]. Fig. 4e shows the schematic diagram of the fracture mechanism of IMCs under UVT. The larger grains in the raw crystallized MGs are instantaneously reduced to less than 5 nm in localized areas after UVT treatment. When the grains are reduced to a size dominated by the slip deformation mechanism [39], cracks tend to easily form nanovoid at the GB sliding triple junction [42]. These nanovoids will then become the core of intergranular cracks and grow [42,43] further under the action of UVT. The GBs brittleness is also an inherent property of most IMCs, which contributes to crack nucleation at GBs [43].

On the other hand, the ultra-fine grain structure also promotes the process of crack propagation. Its main mechanism is to reduce the deflection of crack paths with smaller grains [44]. The nanocrystals show relatively flat crack paths compared to the coarse crystalline material [39,44]. In this work, the already existing nanograins in crystallized MGs and the continuous grain refinement process leads to instant crack propagation to fracture.

#### 4. Conclusions

In this work, an efficient and less-cost method was discovered to fabricate ultra-fine grain IMC powders. By UVT, we successfully crushed 6 kinds of high-strength bulk crystallized MGs to fine size at room temperature and low stress, and investigated the crushing mechanism. The experimental results show that UVT refines the grains on the contact surface at a rapid rate and induces cracks to nucleate at the GB sliding triple junction. In addition, the ultra-fine grain state greatly shorten the crack diffusion path. This method developed in this paper provides a breakthrough new strategy for the rapid manufacturing of IMC powders.

#### Author statement

Luyao Li: Methodology, Investigation, Formal analysis, Writing – Original Draft, Visualization. Wenxin Wen: Methodology, Formal analysis. Jinbiao Huang: Formal analysis. Jianan Fu: Methodology, Investigation, Formal analysis. Jiang Ma: Conceptualization, Resources,

Writing – Review & Editing, Funding acquisition, Supervision.

#### Declaration of competing interest

The authors declare that they have no known competing financial interests or personal relationships that could have appeared to influence the work reported in this paper.

#### Data availability

Data will be made available on request.

#### Acknowledgements

The work was supported by the Key Basic and Applied Research Program of Guangdong Province, China (Grant Nr. 2019B030302010), the NSF of China (Grant Nr. 52122105, 51871157, 51971150), the National Key Research and Development Program of China (Grant No. 2018YFA0703604). The authors also thank the useful discussions with Prof. Y.H. Liu and the assistance on microscope observation received from the Electron Microscope Center of the Shenzhen University.

#### Appendix A. Supplementary data

Supplementary data to this article can be found online at <https://doi.org/10.1016/j.intermet.2022.107672>.

#### References

- [1] S. Scudino, G. Liu, M. Sakaliyska, K.B. Surreddi, J. Eckert, Powder metallurgy of Al-based metal matrix composites reinforced with  $\beta$ -Al<sub>3</sub>Mg<sub>2</sub> intermetallic particles: analysis and modeling of mechanical properties, *Acta Mater.* 57 (2009) 4529–4538.
- [2] A.K. Vivekanandan, B. Muthukutti, S.-M. Chen, M. Sivakumar, S.-H. Chen, Intermetallic compound Cu<sub>2</sub>Sb nanoparticles for effective electrocatalytic oxidation of an antibiotic drug: sulphadiazine, *ACS Sustain. Chem. Eng.* 8 (2020) 17718–17726.
- [3] L.E.R. Vega, D.R. Leiva, R.M.L. Neto, W.B. Silva, R.A. Silva, T.T. Ishikawa, C. S. Kiminami, W.J. Botta, Mechanical activation of TiFe for hydrogen storage by cold rolling under inert atmosphere, *Int. J. Hydrogen Energy* 43 (2018) 2913–2918.
- [4] F. Popa, I. Chicinas, O. Isnard, AlSb intermetallic semiconductor compound formation by solid state reaction after partial amorphization induced by mechanical alloying, *Intermetallics* 93 (2018) 371–376.
- [5] S. Moustafa, W. Daoush, Synthesis of nano-sized Fe–Ni powder by chemical process for magnetic applications, *J. Mater. Process. Technol.* 181 (2007) 59–63.
- [6] B. Glowacki, M. Majoros, M. Vickers, J. Evetts, Y. Shi, I. McDougall, Superconductivity of powder-in-tube MgB<sub>2</sub> wires, *Supercond. Sci. Technol.* 14 (2001) 193.
- [7] Y. Chen, D. Liang, X.P. Gao, J.L.D. Alexander, Sensing and energy harvesting of fluidic flow by InAs nanowires, *Nano Lett.* 13 (2013) 3953–3957.
- [8] P. Yadav, Z. Fu, M. Knorr, N. Travitzky, Binder jetting 3D printing of titanium aluminides based materials: a feasibility study, *Adv. Eng. Mater.* 22 (2020), 2000408.
- [9] L.Y. Chen, S.X. Liang, Y. Liu, L.C. Zhang, Additive manufacturing of metallic lattice structures: unconstrained design, accurate fabrication, fascinated performances, and challenges, *Mater. Sci. Eng. R Rep.* 146 (2021), 100648.
- [10] A.V. Korznikov, Z. Pakiel, K.J. Kurzydowski, Influence of long-range ordering on mechanical properties of nanocrystalline Ni<sub>3</sub>Al, *Scripta Mater.* 45 (2001) 309–315.
- [11] Y. Yan, J.S. Du, K.D. Gilroy, D. Yang, Y. Xia, H. Zhang, Intermetallic nanocrystals: syntheses and catalytic applications, *Adv. Mater.* 29 (2017), 1605997.
- [12] P. Zhou, J. Xie, Y. Liu, L. Deng, Composition dependence of microstructure, magnetic and microwave properties in ball-milled FeSiB nanocrystalline flakes, *J. Magn. Magn. Mater.* 320 (2008) 3390–3393.
- [13] G. Herzer, Modern soft magnets: amorphous and nanocrystalline materials, *Acta Mater.* 61 (2013) 718–734.
- [14] L. Cao, Z. Zhao, Z. Liu, W. Gao, S. Dai, J. Gha, W. Xue, H. Sun, X. Duan, X. Pan, Differential surface elemental distribution leads to significantly enhanced stability of PtNi-based ORR catalysts, *Mater* 1 (2019) 1567–1580.
- [15] R.M. Castagna, J.M. Sieben, A.E. Alvarez, M.D. Sanchez, M.M. Duarte, Carbon supported PtNiCu nanostructured particles for the electro-oxidation of ethanol in acid environment, *Mater. Today Energy* 15 (2020), 10036.
- [16] L.C. Zhang, Z. Jia, F. Lyu, S.X. Liang, J. Lu, A review of catalytic performance of metallic glasses in wastewater treatment: recent progress and prospects, *Prog. Mater. Sci.* 105 (2019), 100576.

- [17] R.J. Voorhoeve, J. Remeika, P. Freeland, B. Matthias, Rare-earth oxides of manganese and cobalt rival platinum for the treatment of carbon monoxide in auto exhaust, *Science* 177 (1972) 353–354.
- [18] M. Ozawa, Thermal stabilization of catalytic compositions for automobile exhaust treatment through rare earth modification of alumina nanoparticle support, *J. Alloys Compd.* 408 (2006) 1090–1095.
- [19] Z. Xu, C. Smith, S. Chen, J. Sankar, Development and microstructural characterizations of Mg–Zn–Ca alloys for biomedical applications, *Mater. Sci. Eng. B* 176 (2011) 1660–1665.
- [20] N. Salah, S.S. Habib, Z.H. Khan, A. Memic, A. Azam, E. Alarfaj, N. Zahed, S. Al-Hamed, High-energy ball milling technique for ZnO nanoparticles as antibacterial material, *Int. J. Nanomed.* 6 (2011) 863.
- [21] A. Bor, B. Jargalsaikhan, K. Uranchimeg, J. Lee, H. Choi, Particle morphology control of metal powder with various experimental conditions using ball milling, *Powder Technol.* 394 (2021) 181–190.
- [22] R. Rajkhowa, L. Wang, X. Wang, Ultra-fine silk powder preparation through rotary and ball milling, *Powder Technol.* 185 (2008) 87–95.
- [23] S. Lagutkin, L. Achelis, S. Sheikhaliev, V. Uhlenwinkel, V. Srivastava, Atomization process for metal powder, *Mater. Sci. Eng.* 383 (2004) 1–6.
- [24] D. Beckers, N. Ellendt, U. Fritsching, V. Uhlenwinkel, Impact of process flow conditions on particle morphology in metal powder production via gas atomization, *Adv. Powder Technol.* 31 (2020) 300–311.
- [25] B. Liu, H. Gu, Q. Chen, Preparation of nanosized Mo powder by microwave plasma chemical vapor deposition method, *Mater. Chem. Phys.* 59 (1999) 204–209.
- [26] K. Sahnner, M. Kaspar, R. Moos, Assessment of the novel aerosol deposition method for room temperature preparation of metal oxide gas sensor films, *Sensor. Actuator. B Chem.* 139 (2009) 394–399.
- [27] T. Wang, D.-C. Sun, Preparation and characterization of nanometer-scale powders ceria by electrochemical deposition method, *Mater. Res. Bull.* 43 (2008) 1754–1760.
- [28] G. Orhan, G. Hapçı, Effect of electrolysis parameters on the morphologies of copper powder obtained in a rotating cylinder electrode cell, *Powder Technol.* 201 (2010) 57–63.
- [29] R.K. Nekouie, F. Rashchi, N.N. Joda, Effect of organic additives on synthesis of copper nano powders by pulsing electrolysis, *Powder Technol.* 237 (2013) 554–561.
- [30] S. Jiao, H. Zhu, Electrolysis of Ti<sub>2</sub>CO solid solution prepared by TiC and TiO<sub>2</sub>, *J. Alloys Compd.* 438 (2007) 243–246.
- [31] Z. Wang, J. Tan, B. Sun, S. Scudino, K. Prashanth, W. Zhang, Y. Li, J. Eckert, Fabrication and mechanical properties of Al-based metal matrix composites reinforced with Mg<sub>65</sub>Cu<sub>20</sub>Zn<sub>5</sub>Y<sub>10</sub> metallic glass particles, *Mater. Sci. Eng.* 600 (2014) 53–58.
- [32] J. Ma, C. Yang, X. Liu, B. Shang, Q. He, F. Li, T. Wang, D. Wei, X. Liang, X. Wu, Fast surface dynamics enabled cold joining of metallic glasses, *Sci. Adv.* 5 (2019), eaax7256.
- [33] X. Li, D. Wei, J. Zhang, X. Liu, Z. Li, T. Wang, Q. He, Y. Wang, J. Ma, W. Wang, Ultrasonic plasticity of metallic glass near room temperature, *Appl. Mater. Today* 21 (2020), 100866.
- [34] Z. Huang, J. Fu, X. Li, W. Wen, H. Lin, Y. Lou, F. Luo, Z. Zhang, X. Liang, J. Ma, Ultrasonic-assisted rapid cold welding of bulk metallic glasses, *Sci. China Mater.* 65 (2022) 255–262.
- [35] Z. Li, X. Li, Z. Huang, Z. Zhang, X. Liang, H. Liu, P.K. Liaw, J. Ma, J. Shen, Ultrasonic-vibration-enhanced plasticity of an entropic alloy at room temperature, *Acta Mater.* 225 (2022), 117569.
- [36] Z. Huang, D. Wagner, C. Bathias, P.C. Paris, Subsurface crack initiation and propagation mechanisms in gigacycle fatigue, *Acta Mater.* 58 (18) (2010) 6046–6054.
- [37] F. Dalla Torre, P. Spätig, R. Schäublin, M. Victoria, Deformation behaviour and microstructure of nanocrystalline electrodeposited and high pressure torsioned nickel, *Acta Mater.* 53 (2005) 2337–2349.
- [38] Y.T. Zhu, T.G. Langdon, Influence of grain size on deformation mechanisms: an extension to nanocrystalline materials, *Mater. Sci. Eng.* 409 (2005) 234–242.
- [39] P. Cavaliere, Fatigue properties and crack behavior of ultra-fine and nanocrystalline pure metals, *Int. J. Fatig.* 31 (2009) 1476–1489.
- [40] D. Jang, M. Atzmon, Grain-size dependence of plastic deformation in nanocrystalline Fe, *J. Appl. Phys.* 93 (2003) 9282–9286.
- [41] J.R. Trelewicz, C.A. Schuh, The Hall–Petch breakdown in nanocrystalline metals: a crossover to glass-like deformation, *Acta Mater.* 55 (2007) 5948–5958.
- [42] A. Sheinerman Ovid'ko, Triple junction nanocracks in deformed nanocrystalline materials, *Acta Mater.* 52 (2004) 1201–1209.
- [43] V. Vitek, S. Chen, Modeling of grain boundary structures and properties in intermetallic compounds, *Scripta Metall.* 25 (1991).
- [44] T. Hanlon, E. Tabachnikova, S. Suresh, Fatigue behavior of nanocrystalline metals and alloys, *Int. J. Fatig.* 27 (2005) 1147–1158.